Original papers

Hydrodynamics of Atlantic salmon culture tank: Effect of inlet nozzle angle on the velocity field

J.M.R. Gorle[a,*], B.F. Terjesen[a,1], S.T. Summerfelt[b,2]

[a] *Nofima AS, Sunndalsøra 6600, Norway*
[b] *The Conservation Fund Freshwater Institute, 1098 Turner Road, Shepherdstown, WV 25443, USA*

A B S T R A C T

The aquaculture industry is increasingly interested in using larger rearing tanks of near $1000\,m^3$ to achieve production and economic benefits. Higher Reynolds number due to that order of tank size makes the flow fully turbulent. This paper presents a full-scale computational fluid dynamics (CFD) model of an existing culture tank of $788\,m^3$ size was developed, based on time-dependent incompressible unsteady Reynolds averaged Navier-Stokes (URANS) formulation with the realizable k-ε viscous model. The tank has two inlet pipes, placed closed to side walls of the tank. Each pipe has 11 inlet nozzles, which introduce the flow into the tank parallel to the walls. This base case was validated against the experimental velocity measurements using Acoustic Doppler Velocimetry (ADV) at predefined locations across the central vertical plane of the tank.

Turbulence characteristics and hence the hydrodynamic performance of the tank are influenced by inflow characteristics. To conclude this, two redesigns were developed and contrasted with the base design for various flow parameters from the viewpoint of the tank's performance. Redesign 1 has the nozzles turned towards the centre by 42°, while Redesign 2 has bottom 5 nozzles directing the flow towards the centre with the rest injecting the flow parallel to the wall. Distribution of turbulence parameters and vortices reveal that the inflow with a radial component improves the mixing and flow uniformity characteristics of the tank. The present study has shown that relatively minor construction changes aided by CFD can result in major changes in the hydrodynamic properties of large culture tanks for Atlantic salmon.

1. Introduction

Recirculating Aquaculture System (RAS), unlike conventional single-pass culture systems, provides a controlled environment that uniquely favours fish welfare and operational performance (Dalsgaard et al., 2013; Summerfelt et al., 2016). There is currently considerable interest in land-based and sea-based closed-containment systems for salmon post-smolts (Terjesen et al., 2013), with tank volumes up to several thousand cubic meters. Rather than conducting theoretical and experimental investigations on such large fluidic systems, it is more efficient to use appropriate computational models for assessing the flow and structural properties. Computational studies with transient turbulence solvers, thanks to high-end computing capabilities, can enhance the scope of process design and performance optimization. This can save enormous labour and time. However, given the relatively limited scope of the literature available on the computational models of culture

tank hydrodynamics for performance metrics, the present-day aquaculture industry is largely relying on laws of similarity and past experience. Although it is reliable, dimensioning the large RAS tanks for nominal design configurations and operating conditions for the given phase of the fish life cycle cannot provide accurate information about flow pattern. Such methodology simply misses the opportunity to optimize the tank's performance and quality aspects of the working fluid.

In the context of the application of larger culture tanks for reduced costs, optimum tank design is of paramount interest to achieve desired flow conditions in the tank (Farghally et al., 2014; Elalouf et al., 2018). However, the hydrodynamic performance of tanks, both circular and octagonal, is vulnerable to the inherent turbulence and velocity profiles created by different geometries, internal structures for flow injection and removal, and fish biomass. For Atlantic salmon parr, smolt, and post-smolt, research suggests that the ideal swimming speed is approximately 1–1.5 body lengths per second to improve growth rate,

---

Nomenclature

A	area (m^2)
C_1, C_2, C_3, C_μ	model constants of the realizable $k - \varepsilon$ model
h	water column height in the tank (m)
k	turbulent kinetic energy (m^2/s^2)
p	pressure (pa)
P_k and Y_m	production and dissipation terms of turbulence
R	radial distance from tank's centre (m)
Re	Reynolds number
S_{ij}	strain rate tensor
u	local velocity (m/s)
U	inlet velocity (m/s)
$y+$	non-dimensional wall distance

Greek symbols

$\propto$	flow angle (rad)
β	Eddy viscosity ratio
γ	flow uniformity index
δ	Kronecker Delta
ε	dissipation rate of turbulent kinetic energy (m^2/s^3)
θ	dihedral angle of the cells (°)
μ	water viscosity (Pa.s)
μ_t	turbulent viscosity (Pa.s)
ν	kinematic viscosity of water (m^2/s)
ρ	water density (kg/m^3)
Φ	arbitrary flow variable
$\bar{\Phi}$ and Φ'	mean and fluctuating components of the variable 'Φ'

Abbreviations

ADV	Acoustic Doppler Velocimetry
CAD	Computer aided design
CFD	Computational fluid dynamics
HRT	Hydraulic retention time
LES	Large eddy simulation
RAS	Recirculating aquaculture system
STEP/STP	Standard for the exchange of product data
TKE	Turbulent kinetic energy
URF	Under-relaxation factor

disease resistance, and general robustness (Davison, 1997; Castro et al., 2011). Also, consider that the primary rotating flow creates the secondary radial flow, and these velocity components combine to create a self-cleaning tank without dead-zones, i.e. regions where typical hydraulics are suppressed, were settleable solids can accumulate. A water velocity of 15–30 cm/s across the floor of the tank is suggested to prevent biosolids and most feed from accumulating (Timmons et al., 1998). In addition to particle settling, hydrodynamics in circular and octagonal tans should promote uniform mixing to create near homogeneous concentrations of dissolved metabolites (e.g., O_2, CO_2, TAN). For example, concentration gradients in dissolved oxygen within intensive circular culture tanks can be typically maintained at less than approximately ± 1 mg/L about the mean (typically 90–100% saturation) tank concentration (Davidson and Summerfelt, 2004; Gorle et al., 2018b). In addition, diverse design parameters such as tank size and shape, location and dimensions of inlets and outlets etc. (Summerfelt et al., 2016), and operating conditions including flow velocity at inlet and exit, water head, and functional parameters including impulse force, tangential and radial velocity components, Reynolds number etc. (Davidson and Summerfelt, 2004; Oca and Masalo, 2013; Venegas et al., 2014; Prabhu et al., 2017; Gorle et al., 2018b) characterize the hydrodynamic behaviour of the tanks. Appropriate design of larger culture tanks should appraise 3D flow effects, velocity and pressure gradients and vortex dynamics (Lee, 2015; Shi et al., 2017), which add additional complexity to the system. Developing the computational models of such large culture tanks is not straightforward due to the presence of multiple solid boundaries and prevailing flow nonlinearities. Therefore, an acceptable solution with defendable assumptions is usually sought.

Uniform flow distribution for effective feed distribution and sufficient mixing for desirable water quality are major concerns in the design and operation of a culture tank. Higher flow rates are used to ensure uniform water quality, which requires the optimal design of the inlet and outlet structures for effective water exchange, feeding rate, waste production and energy consumption (Prehn et al., 2012; Carvalho et al., 2013; Shete et al., 2016). Effect of inflow configuration on the overall flow performance in closed domains has been widely studied in other types of applications. For instance, Ostermeier et al. (2017) studied the effect of nozzle geometry on flow distribution in the application of solid-gas fluidized beds, and Tang et al. (2017) examined the inlet design on the properties of a hydrocyclone. Although a pure tangential inflow is considered as the easiest and most economical

technique of producing a rotating flow in a culture tank (Timmons et al., 1998), other inlet conditions have been tested on occasions. For example, adjustable inlet nozzles were employed by Davidson and Summerfelt (2004) for assessing the performance of Cornell-type dual-drains in a circular tank. A similar technique was used by Summerfelt et al. (2004) in studies on a partial reuse system for cold water aquaculture. The experiments on raceway hydrodynamics by Labatut et al. (2007) revealed that the characteristics of inlet along with outlet influence the flow velocity and uniformity. Such studies on inlet characteristics miss the basal technical causatory explanations, and hence an extensive investigation is necessary. However, this needs to take into account that the flow injection mechanism should be able to solve or minimize the existing hydraulic problems, for a given set of design and operating conditions.

In regard to the flow dynamics and mixing action occurring in the culture tanks, where the flow pattern is circular and the outlet is located at the centre, the concepts of 'teacup hydrodynamics' and 'columnar vortex' are invaluable. While the former was adequately discussed by the scholars in the context of culture tank hydrodynamics (Timmons et al., 1998; Davidson and Summerfelt, 2005; Plew et al., 2015), the vorticity distribution across the tank has been ignored. Summerfelt et al. (2016) reported that the mean hydraulic retention time in commercial culture tanks vary between 35 and 53 min, which gives an optimal rotational flow. While it was demonstrated that good water mixing could be achieved within this practical range of hydraulic retention times (HRT), no study has been performed to account for the variations of field variables at different flowrates.

Simulation-based design improvement and optimization is a new frontier in the field of aquaculture due to the possibility to embed the modifications into 3D geometries. There has been an increasing interest in developing new designs of rearing facilities due to the currently major innovations in production methods used in salmon aquaculture, motivated by challenges with sea-based traditional methods. Cage systems were computationally modelled by Kim et al. (2015) to study the effect on the growth rate of marine animals. Cornejo et al. (2014) developed a large eddy simulation (LES) model of a similar domain to examine the wake properties. A handful of computational studies were performed on raceways to investigate discharge methods (Labatut et al., 2015), and sediment transport (Huggins et al., 2004, 2005; Stockton et al., 2016). Very few studies, however, have been conducted on the flow dynamics of a RAS environment. For instance, a general hydrodynamic analysis of an octagonal RAS tank, using the realizable k-ε

viscous solver was performed by Liu et al. (2017a), and the effect of flow split between outlets of a culture tank with Cornell-dual drain system on the turbulence field was computationally studied by Gorle et al. (2018c). Therefore, a knowledge gap exists in the improvement or optimization of the design of RAS tanks. In the present study, hydrodynamics of a commercial RAS tank in operation was investigated at full-scale using turbulence modelling. Although the practical experience at farms highlights several issues related to tank hydrodynamics such as vortices, flow uniformity, energy losses, and turbulence, these aspects lacked a high-fidelity analysis in the existing literature. The novelty of the present study lies in the computation of Q-criterion for coherent vortical structures at practical operating conditions, γ-index for flow uniformity, walls shear stresses for energy loss, and non-dimensional turbulent kinetic energy and its dissipation rate for hydrodynamic turbulence in the tank. Flow evaluation of this base design of the tank is then followed by the redesign of nozzle configuration to quantify the effect of inflow direction on the global hydrodynamic pattern.

2. Recirculation aquaculture system (RAS) tank under study

The design and flow conditions were investigated in a 788 m^3 size octagonal RAS tank at Marine Harvest ASA, Steinsvik in Norway, where Atlantic salmon smolts were reared. The site has two RAS systems, each having six tanks, which are identical in design but different in operating conditions. Fig. 1(a-c) show the design and basic dimensions of the tank and outlet system. The tank is equipped with two identical inlet pipes of 45 cm diameter, placed at a distance of 40 cm from the nearest side wall. Each inlet pipe has 11 nozzles of size 9 cm each. The direction of the inflow is parallel to the walls so that the flow pattern is clockwise when viewed from the top. Although the wall height of the tank is 4.2 m, the water level is maintained at 3.9 m height. Conical tank design promotes better mixing of solid particles with the flow and thereby self-cleaning ability (Carvalho et al., 2013). The 10° inclined conical base, which draws the solid particles to the centre, promotes the formation of secondary vortices. The solid particles in the flow are therefore mixed and entrained in this location. This becomes more intensive with higher vortex strength, which primarily depends on operating conditions.

The manual operation of valves on the inlet pipelines used at this RAS facility makes it nearly impossible to maintain the definite and equal inflow rates from the two inlet pipes. While it is usual to have 10–15% difference between the flowrates through the two pipes, this difference could be as high as 30–40%. Unequal flow rates through the inlet pipes in a confined flow domain would cause a highly non-uniform flow pattern. For instance, Fig. 2(a) shows the CFD-assisted streamline pattern in the tank when Inlet 1 supplies 25% more flow than the Inlet 2 with a mean hydraulic retention time of 45 min. In order to avoid the skewed flow pattern in the tank as well as prevent the formation of dead zones near the centre, the outlet casing was modified with two openings, as shown in Fig. 1(c), which allow the tank flow to disregard the vertical pipes but pass into the central outlet casing and get out of the tank. The resulting circular flow pattern is shown in Fig. 2(b). In the modified outlet, the casing influences the distribution of secondary vortices, which occur in the vertical planes. As shown in Fig. 2(c) and (d), the absence of flow through the casing preserved the coherence of the secondary vortex, which was broken in the other case. The strength of secondary vortices is one of the important factors that create the mixing action in the flow whereby the solid particles are likely carried away by the stream without sedimenting, and thus ensure homogeneous water quality in the tank (Gorle et al., 2018b). One of the objectives is therefore to obtain the advantages of both cases; a globally uniform flow with strong coherent secondary vortices.

3. Methodology

3.1. Experimental setup

A Nortek high-resolution acoustic Doppler profiler, *Vector*, for velocity measurements in the tank. The working principle of the device is based on the Doppler shift, which accounts for the effect of a moving fluid element on the frequency of the acoustic waves that the device emits, whereby the wavelength is shortened as the distance between the source moves towards the target element and lengthened as it moves away (Neipp et al., 2003). Acoustic Doppler Velocimetry (ADV) system consists of a processing module that houses the control and signal conditioning electronics, and a shaft that contains the signal transmitter and receiver. Calculation of velocity components takes into account the difference between the transmitter frequency and receiver frequency. The three-legged instrument emits the beams with a separation angle between each other of 120° on the horizontal plane and each beam makes a vertical angle of 25°. The target volume is a cylindrical water element, which was at 10 cm from the transmitter. The schematic diagram of the ADV unit is shown in Fig. 3(a).

A rectilinear coordinate system was created for velocity measurements in the tank, as depicted in Fig. 3(b). The origin was located at (0,
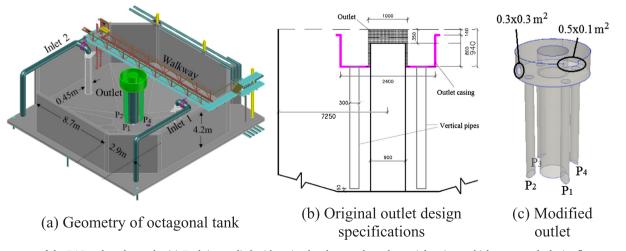

(a) Geometry of octagonal tank

(b) Original outlet design specifications

(c) Modified outlet

Fig. 1. Geometry of the RAS tank under study. (a) Tank is supplied with recirculated water through two inlet pipes, which create a clockwise flow pattern when viewed from the top. Walkway allows for velocity measurements to generate the velocity profile across the central vertical plane. (b) Water is collected to the outlet through four vertical pipes at the tank's centre, and (c) The modified outlet design has two openings on the casing, which get approximately 40% of water directly to the outlet boundary from the tank. Also, angled bottom creates more suction area for the water, which limits the rupturing of solid particles.
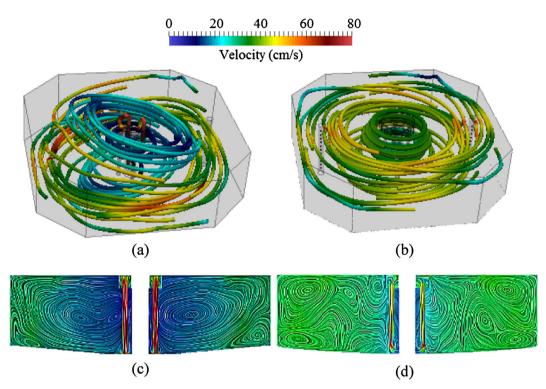
Fig. 2. Streamline pattern in the tank with 25% more inflow from Inlet 1 than Inlet 2. The total flow rate is 292 L/s. (a) and (b) show 3D streamlines without and with flow through the outlet casing, and (c) and (d) sectional streamline distribution across the central vertical plane without and with flow through the outlet casing, respectively.
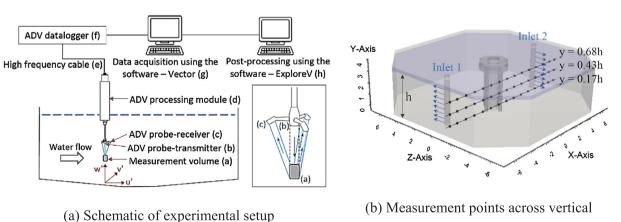
0, −1.5) in the laboratory frame. Fifteen measurement points at each of three depths constitute the complete measurement plane. The ADV technique requires the transmitter head to be placed in the water. Because the velocity measurements close to bottom are likely influenced by the solid surface (Guerra and Thomson, 2017), the lowest depth for measurements was kept at 17% of wall height. Also, the velocities close to the free-surface cannot be accurately measured by ADV, which limited placement of the upper measurement line at 68% of wall height. The resulting 15×3 measurements were used to validate the computational results.

3.2. Computational framework

CFD application, in spite of being an exhaustive field, of interdisciplinary nature of modelling and improving aquaculture systems invokes the need for an integrated computational framework. This consists of diverse tools and techniques for evaluation of the flowfield and quantity based investigation. The present study established a five-step framework as illustrated below.

1. *Development of CAD model.* CATIA V5 (Dassault Systems, France) was used to create the geometries in STEP/STP format.
2. *CAD translation.* The required format for the computer simulations was Parasolid. Therefore, an external CAD transformation tool, called 3D-Tool (3D-Tool GmbH & Co. KG, Germany) was used to convert the STEP/STP file into a .X_T file.
3. *Meshing.* An automated meshing process was performed using the tool, Castnet (DHCAE Tools GmbH, Germany) to create hybrid grids

(a) Schematic of experimental setup

(b) Measurement points across vertical plane, z = -1.5 m

Fig. 3. Acoustic Doppler Velocimetry (ADV) setup for the velocity measurement in the tank including data flow from the measurement tier to post-processing unit. The signal from the transmitter to the receiver is shown in the inset. (b) Velocity measurement points at three depths in the tank. Arrows from the inlet pipes shows the direction of inflow, which is parallel to the nearest wall. The water level was maintained at $h = 3.9$ m.

to solve the conservation equations.

4. *Solution process*. BlueCFD (blueCAPE, Portugal) which is a finite volume software, based on OpenFOAM technology, was implemented to solve the conservation equations.

5. *Post-processing*. Paraview (Kitware, USA) and Matlab (Mathworks, USA) were used to plot and visualize the results.

Referring to Fig. 1(a), the geometry of the water body with a column height of 3.9 m, was sufficient to investigate the hydrodynamics in the tank. Therefore, unnecessary structures such as walkway, piping and supporting elements outside of the water column were eliminated from the CAD environment. Although care was taken, inevitable uncertainties in replicating the exact geometry of 788 m³ volume were expected to cause a minor deviation of computational results from the experimental findings.

3.2.1. Domain discretization

The numerical analysis of the RAS tank in the present case involves the decomposition of the entire flow domain into a number of control volumes or cells. The complex sub-geometries in the model require a flexible cell distribution for better solution accuracy. However, an unstructured cell distribution requires more computational time and storage space (Ito, 2013). The present 3D study, therefore, used a hybrid formulation; unstructured triangular meshing on the solid surfaces and structured hexahedral cells in the core. Tetrahedral cells are used to connect these two zones. Fig. 4(a) shows the unstructured surface mesh across the geometry. Fig. 4(b) shows the mesh visualization on the vertical cut section through tank's centre. While effectively negotiating the complex and small geometrical features, such semi-structured mesh retains robust tracking of spatial and temporal flow characteristics as well as enables the interpolation of field variables for better analysis (Sarrate et al., 2014; Liu et al., 2017b). The flowfield is more complex within approximately 1.5 m radius from the tank's centre due to the presence of the central outlet system. In addition to the directional change of the flow, this region experiences more dynamic behaviour, such as an accelerated flow at the bottom of vertical pipes, recirculation in the pipes, strong vortex distribution in the casing, flow exit through the outlet, etc. A local refinement in this region is necessary to capture the flow variations more accurately. A cylindrical mesh control was therefore used to refine this region, where the mesh density was increased by 50% through the insertion of hexahedral cells, and grid connectivity was maintained through tetrahedral cells.

Unstructured grids however require an extra attention towards the mesh quality for better computational accuracy, as demonstrated by Katz and Sankaran (2011). Because the numerical error generated by the cell angles is in proportional to $1/\sin\theta$, the dihedral angle of the
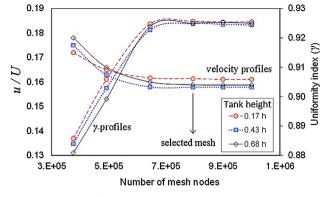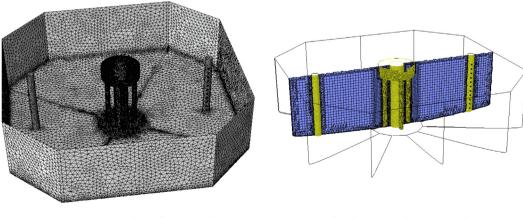

Fig. 5. Mesh sensitivity analysis.

cells, θ, should not be close to either 0° or 180°. The present mesh has 95% of the elements with dihedral angle in the range of [70°, 120°]. Another important criterion that affects the solution convergence is the mesh smoothness. The quality of computational grid in CFD studies is often measured from the skewness and aspect ratio of the cells, which must be kept as low as possible. The grid used in this study had 95% of the elements with skewness below 0.5 and 98% with aspect ratio less than 5. In order to capture the boundary layer region, an appropriate near-wall treatment has to be performed for a chosen turbulence model. Because the Reynolds number (Re) of the tank flow is of the order of 4E6, a high-Re formulation was used to treat the near wall region with non-dimensional wall distance $y+ > 30$. Therefore, *wall functions* were used to model the flow closest to the solid surface (Pope, 2000)

Keeping the same mesh topology, six computational grids were tested to identify the solution dependency on mesh size. Because the flow is confined within the large solid body, it is reasonable to select a global flow variables to examine the mesh dependency. Fig. 5 shows convergence of normalized velocity (u/U), and uniformity index (γ) over the mesh size. For a given flow section A, γ is defined as

$$\gamma = 1 - \int_A \frac{\sqrt{(\bar{u} - u)^2}}{2A\bar{u}} dA$$

where u is the local velocity in the cell and $\bar{u}$ is the average velocity. These parameters were computed across three horizontal planes along the selected measurement lines, shown in Fig. 3(b). The parameters were converged at the size of 'selected mesh' in Fig. 5, which implied that the effect of grid spacing on the solution was eliminated in the calculation domain with 797,819 cells.

(a) Unstructured surface mesh   (b) Structured core mesh

Fig. 4. Computational grid. (a) Unstructured tetrahedral cells on the surface, and (b) structured quadrilateral cells in the core.

3.2.2. Turbulence modelling

The momentum balance through Navier-Stokes equation considers Reynolds averaging i.e., $\Phi_i = \bar{\Phi}_i + \Phi'_i$, where $\bar{\Phi}_i$ and Φ'_i are the mean and fluctuating components of a flow variable, respectively. Therefore, the instantaneous conservation equations with time-averaging become the ensemble-averaged equations. Using Cartesian tensor notation, the mass and momentum equations can be written as

$$\frac{\partial}{\partial x_i}(\rho u_i) = 0$$

$$\frac{\partial}{\partial x_j}(\rho u_i u_j) = -\frac{\partial p}{\partial x_i} + \frac{\partial}{\partial x_j}\left[\mu\left(\frac{\partial u_i}{\partial x_j} + \frac{\partial u_j}{\partial x_i} - \frac{2}{3}\delta_{ij}\frac{\partial u_i}{\partial x_i}\right)\right] + \frac{\partial}{\partial x_j}(\rho \overline{u'_i u'_j})$$

Thus, Reynolds-averaged Navier-Stokes (RANS) equations introduce additional terms $\rho \overline{u'_i u'_j}$ called Reynolds stresses. In order to close the momentum conservation equation, these turbulence effects must be modelled. In Boussinesq approach, the Reynolds stresses are expressed in terms of mean velocity gradients as

$$\rho \overline{u'_i u'_j} = \mu_t\left[\frac{\partial u_i}{\partial x_j} + \frac{\partial u_j}{\partial x_i}\right] - \frac{2}{3}\left(\rho k + \mu_t \frac{\partial u_i}{\partial x_i}\right)\delta_{ij}$$

Because the Reynolds stress terms can be modelled through the computation of turbulent viscosity, this hypothesis results in lesser CPU effort when compared to the complete modelling of Reynolds stresses. Out of numerous turbulence models available to calculate eddy viscosity by solving different transport equations, the present study used the realizable k-ε model because it was proven to produce more accurate results with a well resolved near-wall region for complex flows (Diaz and Hinz, 2015). Here, the Boussinesq hypothesis is respected by using eddy viscosity μ_t, and mean strain tensor to compute the Reynolds stresses as shown below.

$$\rho \overline{u'_i u'_j} = \frac{2}{3}\delta_{ij}\rho k - \mu_t \underbrace{\left(\frac{\partial \bar{u}_i}{\partial x_j} + \frac{\partial \bar{u}_j}{\partial x_i}\right)}_{\text{Strain tensor } (S_{ij})}$$

where k is the turbulent kinetic energy. The conservation equations for k and its dissipation rate ε are:

$$\frac{\partial}{\partial t}\rho k + \frac{\partial}{\partial x_j}(\rho k u_j) = \frac{\partial}{\partial x_j}\left[\left(\mu + \frac{\mu_t}{\sigma_k}\right)\frac{\partial k}{\partial x_j}\right] + P_k - \rho\varepsilon - Y_m + S_k$$

$$\frac{\partial}{\partial t}\rho\varepsilon + \frac{\partial}{\partial x_j}(\rho\varepsilon u_j) = \frac{\partial}{\partial x_j}\left[\left(\mu + \frac{\mu_t}{\sigma_\varepsilon}\right)\frac{\partial \varepsilon}{\partial x_j}\right] + \rho C_1 S_\varepsilon - \rho C_2 \frac{\varepsilon^2}{k + \sqrt{\nu\varepsilon}} + C_{1\varepsilon}C_{3\varepsilon}P_k\frac{\varepsilon}{k} + S_\varepsilon$$

Here, $C_1 = \max\left[0.43, \frac{\eta}{\eta+5}\right]$, and $\eta = \sqrt{2S_{ij}S_{ij}}\frac{k}{\varepsilon}$.

In these transport equations, P_k and Y_m represent the production and

dissipation terms of turbulence, and S_k and S_ε are the user-defined source terms of k and ε, respectively. Thus, the realizability in this two-equation model is enforced by the formulation of μ_t, which confers that C_μ is not a constant but related to the strain tensor. The realizable k-ε model is also considered superior to the standard k-ε as the former accounts for strong streamline characteristics associated with the flow rotations and vortices, which are natural phenomena in the large flow domains like culture tanks.

One of the limitations of this study is the exclusion of biomass in the tank. Literature shows that the stocking density of the order of 60 kg/m³ would reduce the water velocity by 25% (Gorle et al., 2018b). While the flow fluctuations due to the solid structures in the tank could repel the fish (Liao, 2007), school of fish exhibits both slalom motion through coherent Lagrangian vortices and interception with them leads to low- and high-drag propulsive modes (Huhn et al., 2015; Uddin et al., 2015). The dynamics associated with the fish locomotion is a separate topic itself and deserves extensive research to develop the turbulence model. Therefore, the present study did not consider the biomass in the tank.

3.2.3. Solution procedure

The nozzles on inlet pipes, 1 and 2, were defined as velocity inlets with mass flow specification. The outlet boundary was given the outflow condition. The tank walls are specified with the no-slip condition to capture the boundary layer. Free-surface deformation is negligible due to continuous replenishment of water into the tank (Meshkov and Sirotkin, 2013). Considering the CPU effort in modelling the free-surface in large flow domains, we approximated the free-surface as a stress-free wall.

The unsteady incompressible solver with secondary upwind discretization in space and time was used in computations. The convergence criteria were defined to have 1E-5 as minimum per iteration, while 5E-4 was the maximum observed residual value. Because the anisotropic turbulence model of large turbulent domains with 2nd accuracy is prone to diverge (Wright and Easom, 2003; Aubin et al., 2004), the effect of previous iteration on the present was controlled by adjusting the under-relaxation factors (URFs). The solution was started with low URFs for turbulence parameters and increased sufficiently when a stabilized solution was achieved. The computations were performed with a time step of 0.01 s with 30 sub-iterations. A larger time step was likely to diverge the solution with given set of other parameters. Computations were carried out on a 28 core Intel Xeon E5-2683 v3 2.00 GHz workstation.

4. Results

4.1. Model validation

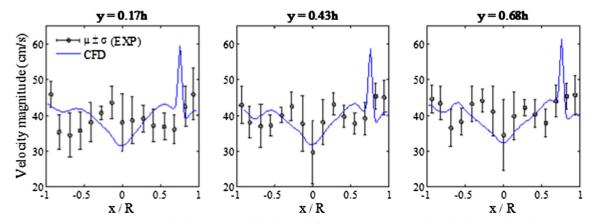Although numerical simulations of general flow physics in full-scale

Fig. 6. Comparison between experimental and computational findings of velocity measurements at three depths across the plane, z = −1.5 m.

industrial applications is vital to address the design issues and further developments, the accuracy of computational results is subject to numerous factors such as the order of discretization, truncation error, uncertainty in the boundary conditions, etc. Because the velocity distribution across the tank is a critical parameter that impacts many factors, from flow uniformity to fish welfare, the developed CFD model was validated against the experimental measurements of velocity magnitude in the tank. In addition to the physical errors in the exact tank dimensioning for modelling purpose, the uncertainties associated with the boundary conditions, fluid properties, and measurement equipment and procedures, significantly affect the model output. As a result, a meaningful validation of the CFD model requires a quantitative valuation of measurement uncertainties to estimate the level of confidence. Fig. 6 shows the comparison between CFD (mean) and ADV (mean ± standard deviation) for velocity datasets at three depths as illustrated in Fig. 3(b). Note that the discrete locations of experimental measurements at different y-locations did not cover the position of inlet jets. The peaks of velocity profiles using CFD at x/R = 0.89 are therefore missing the validation. Although the overall velocity profiles of CFD and ADV follow identical trends, two modes of discrepancy were observed. First, the crests of CFD profiles were at around |x/R| = 0.5, whereas that of ADV were at |x/R| = 0.25. With the prevalence of trough at the tank's centre in both approaches, the CFD-based velocity profiles thus seem elongated. Second, the computational predictions deviate more at greater depths. This complements the fact that the continuous refilling of the tank controls the deformation of water surface (Gorle et al., 2018c), which makes the free-surface relatively lesser influential on the overall hydrodynamic pattern than the deforming free-surface (Yang and Zhou, 2015). Because the CFD predictions are not far from the standard deviation bars of ADV measurements, present computational model supplied a quality solution to analyse the flow and make decisions to improve the system.

4.2. Flowfield analysis

For a computational-based design of a fluidic system, an accurate calculation of convective flow properties plays a vital role in evaluating the flow pattern. Therefore, a descriptive analysis was necessary for the qualitative and quantitative flow parameters, before improving the design. A wide range of turbulence scales generally appears in large flow domains like the present case, with the occurrence of several nonlinear phenomena, like wake formation and vortex motion. In order to assess these 3D flow aspects, gradient-based visualization techniques are used in this study. Using the velocity gradient tensor, a variety of methods were proposed by scholars to locate the vorticity in a flowfield. Using the strain tensor approach, the Q-criterion was evaluated in this study to locate the spatial distribution of vorticity (Haller, 2005). Mathematically, the Q-criterion is defined as the positive second invariant of the velocity curl ($\nabla \times u$) across the flow field (Gorle et al., 2016). When applied to 3D flowfield, Q-representation differentiates the swirling component from pure shear to highlight the coherent vortical structures.
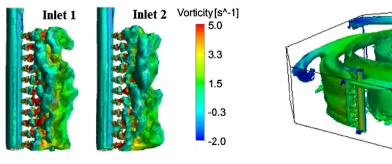
The turbulence associated with the flow through the inlet and across the tank is visualized in Fig. 7 using an iso Q value of 0.005. As the flow is introduced from the nozzles into the tank, it is obvious to have higher velocities near the inlet pipes. In addition, there is a velocity difference between the nozzle stream and the rotating flow in the tank, which creates local shear zones. As a consequence, inlet nozzles become the inherent turbulence generators, as shown in Fig. 7(a). Looking at global flowfield, as described in Fig. 7(b), assisted by Fig. 2(b), it is a flow system that is characterized by nearly concentric streamlines in a circular fluid motion, which is due to tangential inflow in a closed octagonal/circular domain. The resulting vortex column around the central outlet structure is wrapped by the external turbulent filaments, leading to intensive momentum transport. Thus, the vortex column through the interactions with surrounding turbulence reflects on a wide spectrum of turbulent structures prevailing in the domain and affects the dispersion and flushing rates of solid particles (Pumir et al., 2016; Wang and Ohmura, 2017). However, vortex strength beyond a critical value can increase the stress levels of the fish.

In addition, the height of the water column is expected to influence the vortex characteristics in the tank. At higher flow rates and different inflow conditions, there are several possible dynamic actions of vortex column, such as stretching, stripping, buckling, etc. (Candon and Marshall, 2012; Schrottle et al., 2015), which express the complexity associated with the flow. The physics of columnar vortex is however out of the scope of current research.
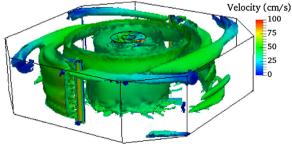
Fig. 8 shows the instantaneous velocity contours at different sections of vertical pipes in the outlet system of the tank. A recirculation zone at the lower part of the pipes is evident, which is due to the change in the flow direction from the tank into the pipes. The flow appears to reattach at about half of the pipe length. From operation's viewpoint, this needs to be sufficiently high i.e. at least 60 cm/s to transport biosolids through the pipes (Terjesen et al., 2013) and overcoming the settling velocity of fish feed. In the existing design, flow through the vertical pipes moves with an average velocity of 63 cm/s. An important functional criterion of the hydrodynamic design is that the pipes carry equal amounts of the flow to the outlet chamber for uniform flow conditions in the chamber and further downstream.

4.3. Effect of inlet nozzle angle

Two different inlet configurations are evaluated to understand the effect of radial inflow on the large culture tank's hydrodynamic behaviour. Fig. 9(a) and (b) show the inlet configurations of the redesigns. Redesign 1 has the inlet nozzles turned into the tank such that the jets were directed to the centre of approaching wall. In Redesign 2, bottom five nozzles are directed to the centre while the top six nozzles retained the same positioning. Thus, the pure tangential inflow in base design, which is the primary contributor to the rotational flow pattern, is partly

(a) Vorticity field near the inlet nozzles

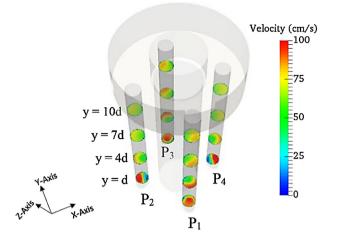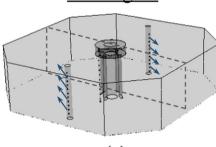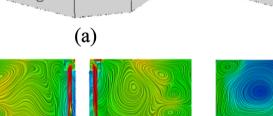(b) Vorticity distribution in the tank

Fig. 7. Coherent vortical structures using Q-criterion (Q = 0.005).

Fig. 8. Velocity contours at different sections of vertical pipes. y/d is the non-dimensional height of each section with respect to the tank's bottom, where d is the pipe diameter (= 30 cm). Inlet pipes are on the X-Axis.

replaced by a radial component in the redesigns. Table 1 shows the corresponding inflow components in the three tank designs.
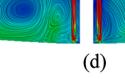
Changing the flow direction in the large water tanks influences both the velocity and vorticity distributions. Effect of the inflow variations in terms of secondary vortex pattern is explained by 2D streamlines across the central vertical plane in Fig. 9(c) and (d) for Redesign 1 and Redesign 2, respectively. It is evidenced that the Redesign 2 produced a continuous and stronger secondary vortex. This is a better condition for improved mixing action, compared to multiple smaller vortices of lower strength, which is the case of Redesign 1. Looking at the fluid motion,
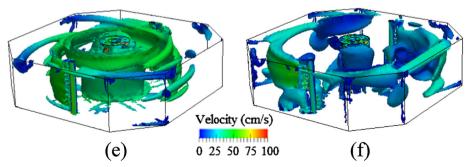
Table 1
Overview of flow components in the three designs.

	Tangential	Diagonal	Radial
Base design	100%	–	
Redesign 1	–	100%	–
Redesign 2	54.5%	–	45.5%

there is a huge difference between the redesigns in terms of vorticity distribution. As shown in Fig. 9(e), diagonal inflow in Redesign 1 has not significantly altered the appearance of the columnar vortex with a little reduction in the intensity, compared to the base design in Fig. 7(b). On the other hand, the formation of intensive swirls is appreciably controlled by the introduction of a radial component to the inflow, as shown in Fig. 9(f). With widely spread vertical structures of low intensity, Redesign 2 ensures more even distribution of turbulence, particularly near the tank walls. Any dead zones, which often occur, near the tank walls and corners are thus controlled in Redesign 2.

The flow structure in the redesigns is first contrasted with the base design for flow angle ($\propto = \tan^{-1}(u_z/u_x)$), which is plotted in Fig. 10. Considering the experimental validation of CFD results, there is a good agreement in terms of absolute flow angle in the case of base design except a reasonable discrepancy near the solid boundaries. This is possibly due to the complexity in capturing the flow physics more accurately around the inlet pipes, close to the tank's floor, where stronger flow gradients and vortex dynamics exist. Turning angle in Redesign 1 is identical to that in base design, which reveals that the flow rotation in the tank is strong enough to overcome the radial flow component, introduced by means of diagonal nozzles. Redesign 2, on the other hand, experienced a drastic variation in the flow angle from the base design.

(a)

(b)

Fig. 9. Two inlet configurations considered for improved flow distribution for a given flow rate. (a) Redesign 1 has the nozzles directing the flow to the centre of approaching face, and (b) Redesign 2 has the upper six nozzles unaltered, but bottom five nozzles directing the flow towards tank's centre. (c) and (d) represent the distribution of corresponding secondary vortices across the central vertical plane of the tank. (e) Redesign 1 exhibits a stronger vortex column around the outlet system, and (f) a broken distribution of columnar vortex occurs in Redesign 2. Coherent vortices in (e) and (f) are presented using Q-criterion using the iso-value of 0.05.
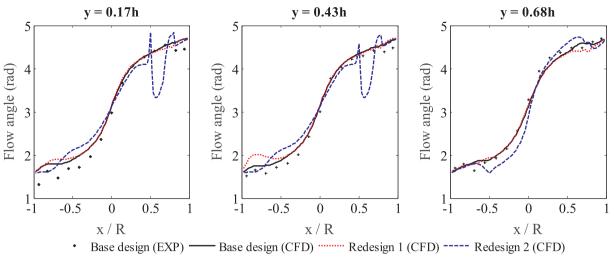

(c)

(d)

(e)

(f)

Fig. 10. Absolute flow angle 'α' along the three measurement lines in the base design and redesigns across z = −1.5.

There was an abrupt drop in the profile of flow angle through the bottom half of the tank along the measurement lines due to the pure radial flow injected from the bottom five nozzles. The influence of this radial inflow from bottom nozzles left the attempt of recovering the shape of flow angle incomplete, which results in a deviating trend, through the upper half of the tank. The effect of these flow structures in redesigns on different parameters is explained henceforth.

Referring to Fig. 11, it is obvious that the higher shear stresses appear on the walls near the jet fronts as in the case of base design and Redesign 1. In contrast, the negotiated flow pattern between the tangential flow from the upper nozzles and radial flow from bottom nozzles of Redesign 2 drastically reduced the average wall stress distribution approximately to one-third. The contours of wall shear stress of the three designs, therefore, suggest that the energy loss in the form of dissipation to the tank walls is less in Redesign 2, compared to the other, which contributes to the flow momentum. The existing design loses the highest amount of flow energy to the walls due to pure tangential inflow.

Fig. 12 presents the flow distribution across the planes y = 0.43 h and y = 0.68 h in the negative z-direction (see Fig. 3b for reference axes), which identifies the spatial variation in the velocity and turbulence parameters. One common feature between the base design and Redesign 1 is that the flow from nozzles is unidirectional. In a confined flow domain with same inlet and outlet conditions, this trait possibly produces identical velocity profiles. On the other hand, 90° angular shift of bottom 5 nozzles in Redesign 2 drastically altered the velocity distribution from the other designs. Also, the near convex trend of normalized velocity in case of Redesign 2 is retained until the flow reaches the wall, whereas it gradually becomes concave in the other two designs.

A common practice in developing the computational models of full-scale industrial systems is to assume isotropic turbulence in the flow domain (Xu et al., 2015; Daddi-Moussa-Ide and Ghaemi, 2015). Since the isotropic homogeneous turbulence decays with time, the transient behaviour of large culture tank hydrodynamics cannot be featured by a simple scalar like eddy viscosity. Eddy viscosity ratio ($\beta = \nu_t/\nu$) is rather regarded as a suitable variable to characterize the eddy transport of momentum in the field. Peak values of β near the inlet nozzles and further downstream represent the higher end of the turbulence spectrum, while the lower values are due to the laminar nature of the flow. It is interesting to notice that the height-wise variation of β near the inlet with Redesign 2 decreases in the downstream. Unlike this, the other two designs exhibit identical β profiles at z = −1, which separate in the downstream direction. Dimensionless turbulent kinetic energy (TKE) plots in the third row, as the first evidence, complement the Fig. 7(a) by showing the sharp peaks near the inlet irrespective to the design. While the TKE profiles of the three designs are more or less identical at z = −1, all of them displayed appreciably different distributions from each other further downstream. An interesting observation is that the Redesign 1, due to unidirectional flow, has lower strain rates than the Redesign 2, which causes the lesser intensity of TKE. This advantage is limited in the case of base design due to higher wall interactions than in Redesign 1. Looking at the non-dimensional dissipation rate of TKE, increased local strain rate in Redesign 2 due to bidirectional flow from the inlet pipe causes higher dissipation than the remaining designs. As the turbulence is concerned, there are meaningful peaks in the profiles near the walls due to higher viscous effects.

Finally, it is important to maintain a balanced amount of flow through the vertical pipes. As understood from Section 4.2 and Fig. 8, outlet casing of base design accounted for approximately 40% of total flow exiting the tank. Ideally, the four vertical pipes would share the remaining flow equally. This is the condition required to prevent the formation of nonuniform flow structures as the flow exits the tank. Table 2 compares the designs for the amounts of flow through the
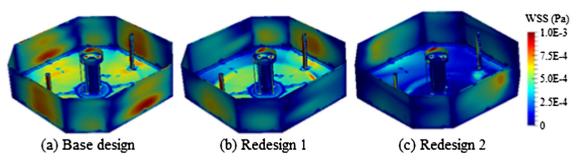

Fig. 11. Comparison of base design with redesigns for wall shear stress distribution.
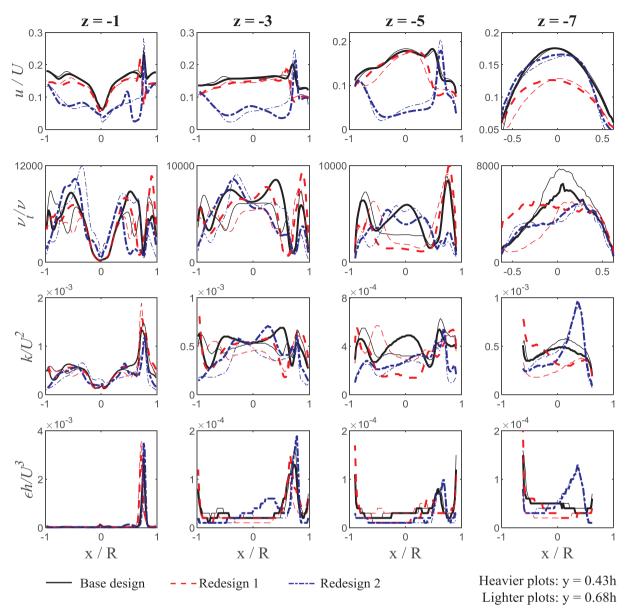
Fig. 12. Comparison of base design and redesigns using the profiles of normalized velocity (1st row), relative eddy viscosity (2nd row), non-dimensional turbulent kinetic energy (3rd row) and its dissipation rate (4th row) at different z-locations.

Table 2

Percent of flow through different exit channels in the three designs. Redesigns are in comparison with the base design without large deviation in the flow exit quantities.

	Base design	Redesign 1	Redesign 2
P_1	15.65	14.92	15.51
P_2	14.70	14.32	14.55
P_3	15.90	15.06	15.55
P_4	14.69	14.34	14.63
Casing	39.06	41.35	39.76

vertical pipes and casing to reach the tank's outlet. With a constant flow supplied in a confined domain, pipes P_1 and P_3 carry more flow than the pipes P_2 and P_4, because former are reached by the inflow faster than the latter. This is more effective when the bottom nozzles inject the flow directly to the centre of the tank, as in the case of Redesign 2. Despite this, the standard deviation in the flow rates through the four vertical pipes is 0.63, 0.60 and 0.54 in base design, and Redesigns 1 and 2, respectively, which admit a more uniform outflow pattern with

Redesign 2.

From the mechanics' perspective, the relationship between the inlet flow rate and the uniformity index is subject to the type of application (for example, Guhan et al., 2016; Zi et al., 2016) depending on the structural design. Although the rotational behaviour of the flow in a RAS tank is analogous to that in mixing tanks, the trend of flow uniformity cannot be compared between them due to the presence of an agitator in the latter (de Lamotte et al., 2017). Higher operating conditions, by means of increasing the flowrate into the tank, enhance the turbulence in the flow domain. Because the vortex dynamics is a major concern in the turbulent energy cascade and vice versa, a parametric study was conducted to understand the effect of flowrate (or mean hydraulic retention time, HRT) on the tank hydrodynamics. Fig. 13 compares the three designs for the vorticity field at different HRTs. While the designed operating condition for 1 kg post-smolt in the selected RAS tank corresponds to an HRT of 45–50 min, two other cases of ± 5 min HRT were considered and the respective distributions of coherent vortices with Q = 0.01 were computed. Irrespective of flowrate, there were two major vorticity features occurring in the flowfield. Firstly, a vertical vortex column around the outlet system, which was
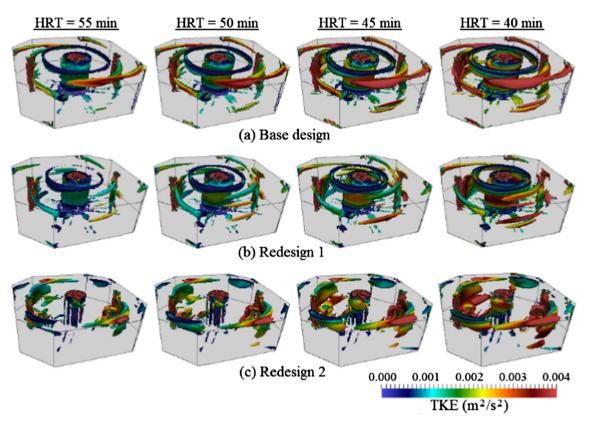
Fig. 13. Pictorial description of the effect of flowrate on the vorticity distribution. 3D renders represent coherent vortical structures using Q = 0.01, coloured with turbulent kinetic energy. Redesign 2 breaks the vortex column around the outlet system and vortical structures were concentrated only near the inlet pipes, which is not the case with other designs.

not allowed to decay irrespective of its interaction with the surrounding turbulence due to the flow confinement. The contour of the columnar vortex was enlarged and registered an increasing intensity of turbulence as flowrate increased. Also, the vortex ring outside of the column near the water surface is stretched by the local strained flow at higher flowrates. This feature was, however, suppressed by the radial inflow in Redesign 2, which implies reduced flow restriction and hence lower stress levels to which the fish could be exposed. Secondly, the external vortical streaks were likely stretched and intensified at higher flowrates. These filaments, which tend to catch up the vortex ring and vortex column, would result in multiscale turbulence interactions. There is an appreciable reduction in the vorticity magnitude as well as turbulence intensity from the existing design to Redesign 1, to Redesign 2, which is certainly due to the induction of radial component in the inflow. As depicted in the case of Redesign 2, the vorticity was more concentrated around the solid surfaces and the turbulence was more quickly dissipated than the other designs. This inference compliments Fig. 12 (row 4), which were the non-dimensional turbulence dissipation profiles along the measurement lines, close to the inlet pipes (at $z = -1.5$).

5. Conclusions

Flow characterization using turbulence models and CFD-based design improvement is useful and yet unexplored techniques in the field of recirculation aquaculture systems (RAS). The maturing technology of RAS, as described by Dalsgaard et al. (2015), still has an ample scope to improve the existing designs using computational methods. This paper presented one such attempt to characterize the hydrodynamics in a large octagonal RAS tank at full scale. With the support of validation experiments using ADV, the merit of 3D CFD model was conveyed through the reproduction of vortical structures and turbulence measurements. The main objective of this study was to improve the existing design for mixing and flow uniformity, which are vital aspects for maintaining homogeneous water quality and preventing biosolids from sedimentation. This was accomplished by testing different inlet nozzle arrangements. We concluded that the inclusion of a radial orientation in the lower flow inlet nozzles would improve the overall hydrodynamic performance of the tank.

Fish faecal matter and denser uneaten feed pellets constitute solids of different material properties and hence different motion profiles in the flow domain. Turbulence external to the columnar vortex has a significant effect on the particle dispersion (Marshall, 2005; Gorle et al., 2018a). Modelling the particle trajectory under the influence of larger eddies such as vortex column should, therefore, resolve the smaller-scale turbulent structures. Flow physics behind such complex phenomena are highly influenced by the hydraulic boundary conditions. Commercial facilities use the standard practice of inlet and outlet locations in the circular tanks. Flow pattern can be changed in a positive way for better mixing and improved uniformity if the flow boundaries are rightly modified.

References

Aubin, J., Fletcher, D.F., Xuereb, C., 2004. Modeling turbulent flow in stirred tanks with CFD: the influence of the modeling approach, turbulence model and numerical scheme. Exp. Therm. Fluid Sci. 28 (5), 431–445. https://doi.org/10.1016/j.expthermflusci.2003.04.001.

Candon, S., Marshall, J.S., 2012. Vortex ring deformation, capture, and entrainment by a columnar vortex. Phys. Fluids 24, 093604. https://doi.org/10.1063/1.4753946.

Castro, V., Helland, B.G., Helland, S.J., Kristensen, T., Jorgensen, S.M., Helgerud, J., Claireaux, G., Farrell, A.P., Krasnov, A., Takle, H., 2011. Aerobic training stimulates growth and promotes disease resistance in Atlantic salmon (Salmo salar). Compar. Biochem. Physiol., Part A 160, 278–290. https://doi.org/10.1016/j.cbpa.2011.06.013.

Carvalho, R.A.P.L.F., Lemos, D.E.L., Taconb, A.G.J., 2013. Performance of single-drain and dual-drain tanks in terms of water velocity profile and solids flushing for in vivo digestibility studies in juvenile shrimp. Aquacult. Eng. 57, 9–17. https://doi.org/10.1016/j.aquaeng.2013.05.004.

Cornejo, P., Sepulveda, H.H., Gutierrez, M.H., Olivares, G., 2014. Numerical studies on the hydrodynamic effects of a salmon farm in an idealized environment. Aquaculture 430, 195–206. https://doi.org/10.1016/j.aquaculture.2014.04.015.

Daddi-Moussa-Ide, A., Ghaemi, A., 2015. Rotation rate of particle pairs in homogeneous isotropic turbulence. Eur. J. Mech. B. Fluids 54, 10–16. https://doi.org/10.1016/j.euromechflu.2015.06.006.

Dalsgaard, J., Lund, I., Thorarinsdottir, R., Drengstig, A., Arvonen, K., Pedersen, P.B., 2013. Farming different species in RAS in Nordic countries: current status and future perspectives. Aquacult. Eng. 53, 2–13. https://doi.org/10.1016/j.aquaeng.2012.11.008.

Dalsgaard, J., Pedersen, L.-F., Pedersen, P.B., 2015. Recirculation technology getting mature. 1–1. Aquacult. Eng. 65. https://doi.org/10.1016/j.aquaeng.2014.12.003.

Davison, W., 1997. The effects of exercise training on Teleost fish, a review of recent literature. Comp. Biochem. Physiol. A Physiol. 117 (1), 67–75. https://doi.org/10.1016/S0300-9629(96)00284-8.

de Lamotte, A., Delafosse, A., Calvo, S., Delvigne, F., Toyea, D., 2017. Investigating the effects of hydrodynamics and mixing on mass transfer through the free surface in stirred tank bioreactors. Chem. Eng. Sci. 172, 125–142. https://doi.org/10.1016/j.ces.2017.06.028.

Davidson, J., Summerfelt, S.T., 2004. Solids flushing, mixing, and water velocity profiles within large (10 and 150 m3) circular 'Cornell-type' dual-drain tanks. Aquacult. Eng. 32 (1), 245–271. https://doi.org/10.1016/j.aquaeng.2004.03.009.

Davidson, J., Summerfelt, S.T., 2005. Solids removal from a coldwater recirculating system comparison of a swirl separator and a radial flow settler. Aquacult. Eng. 33 (1), 47–61. https://doi.org/10.1016/j.aquaeng.2004.11.002.

Diaz, D.D.O., Hinz, D.F., 2015. Performance of eddy viscosity turbulence models for predicting swirling pipe flow: simulations and laser-Doppler velocimetry, arXiv:1507.04648 [physics.flu-dyn].

Elalouf, H., Kaspi, M., Elalouf, A., Halachmi, I., 2018. Optimal operation policy for a sustainable recirculation aquaculture system for ornamental fish: simulation and response surface methodology. Comput. Oper. Res. 89, 230–240. https://doi.org/10.1016/j.cor.2017.05.002.

Farghally, H.M., Atia, D.M., El-madany, H.T., Fahmy, F.H., 2014. Control methodologies based on geothermal recirculating aquaculture system. Energy 78, 826–833. https://doi.org/10.1016/j.energy.2014.10.077.

Gorle, J.M.R., Chatellier, L., Pons, F., Ba, M., 2016. Flow and performance analysis of H-Darrieus hydroturbine in a confined flow: a computational and experimental study. J. Fluids Struct. 66, 382–402. https://doi.org/10.1016/j.jfluidstructs.2016.08.003.

Gorle, J.M.R., Terjesen, B.F., Holan, A.B., Berge, A., Summerfelt, S., 2018a. Qualifying the design of a floating closed-containment fish farm using CFD. Biosyst. Eng. 175, 63–81. https://doi.org/10.1016/j.biosystemseng.2018.08.012.

Gorle, J.M.R., Terjesen, B.F., Mota, V.C., Summerfelt, S., 2018b. Water velocity in commercial RAS culture tanks for Atlantic salmon smolt production. Aquacult. Eng. 81, 89–100. https://doi.org/10.1016/j.aquaeng.2018.03.001.

Gorle, J.M.R., Terjesen, B.F., Summerfelt, S.T., 2018c. Hydrodynamics of octagonal culture tanks with Cornell-type dual-drain system. Comput. Electron. Agric. 151, 354–364. https://doi.org/10.1016/j.compag.2018.06.012.

Guerra, M., Thomson, J., 2017. Turbulence measurements from five-beam acoustic Doppler current profilers. J. Atmos. Oceanic Technol. 34, 1267–1284. https://doi.org/10.1175/JTECH-D-16-0148.1.

Guhan, C.P.O.A., Arthanareeswaran, G., Varadaraja, K.N., Krishnan, S., 2016. Numerical optimization of flow uniformity inside an under body oval substrate to improve emissions of IC engines. J. Comput. Des. Eng. 3 (3), 198–214. https://doi.org/10.1016/j.jcde.2016.02.001.

Haller, G., 2005. An objective definition of a vortex. J. Fluid Mech. 525, 1–26. https://doi.org/10.1017/S0022112004002526.

Huggins, D.L., Piedrahita, R.H., Rumsey, T., 2004. Analysis of sediment transport modeling using computational fluid dynamics (CFD) for aquaculture raceways. Aquacult. Eng. 31 (3–4), 277–293. https://doi.org/10.1016/j.aquaeng.2004.05.007.

Huggins, D.L., Piedrahita, R.H., Rumsey, T., 2005. Use of computational fluid dynamics (CFD) for aquaculture raceway design to increase settling effectiveness. Aquacult. Eng. 33 (3), 167–180. https://doi.org/10.1016/j.aquaeng.2005.01.008.

Huhn, F., VAN Rees, W.M., Gazzola, M., Rossinelli, D., Haller, G., Koumoutsakos, P., 2015. Quantitative flow analysis of swimming dynamics with coherent Lagrangian vortices. Chaos 25, 087405. https://doi.org/10.1063/1.4919794.

Ito, Y., 2013. Challenges in unstructured mesh generation for practical and efficient computational fluid dynamics simulations. Comput. Fluids 85, 47–52. https://doi.org/10.1016/j.compfluid.2012.09.031.

Katz, A., Sankaran, V., 2011. Mesh quality effects on the accuracy of CFD solutions on unstructured meshes. J. Comput. Phys. 230 (20), 7670–7686. https://doi.org/10.1016/j.jcp.2011.06.023.

Kim, T., Yoon, H.-S., Shin, S., Oh, M.-H., Kwon, I., Lee, J., Choi, S.-D., Jeong, K.-S., 2015. Physical and biological evaluation of co-culture cage systems for growout of juvenile abalone, Haliotis discus hannai, with juvenile sea cucumber, Apostichopus japonicus (Selenka), with CFD analysis and indoor seawater tanks. Aquaculture 447, 86–101. https://doi.org/10.1016/j.aquaculture.2014.07.001.

Labatut, R.A., Ebeling, J.M., Bhaskaran, R., Timmons, M.B., 2007. Effects of inlet and outlet flow characteristics on mixed-cell raceway (MCR) hydrodynamics. Aquacult. Eng. 37 (2), 158–170. https://doi.org/10.1016/j.aquaeng.2007.04.002.

Labatut, R.A., Ebeling, J.M., Bhaskaran, R., Timmons, M.B., 2015. Modeling hydrodynamics and path/residence time of aquaculture like particles in a mixed-cell raceway (MCR) using 3D computational fluid dynamics (CFD). Aquacult. Eng. 67, 39–52. https://doi.org/10.1016/j.aquaeng.2015.05.006.

Liao, J.C., 2007. A review of fish swimming mechanics and behaviour in altered flows. Philos. Trans. R. Soc. Lond. B Biol. Sci. 362, 1973–1993. https://doi.org/10.1098/rstb.2007.2082.

Oca, J., Masalo, I., 2013. Flow pattern in aquaculture circular tanks: influence offlowrate, water depth, and water inlet & outlet features. Aquacult. Eng. 52, 65–72. https://doi.org/10.1016/j.aquaeng.2012.09.002.

Lee, J., 2015. Practical applications of low pressure hydrocyclone (LPH) for feed waste and fecal solid removal in a recirculating aquaculture system. Aquacult. Eng. 69, 37–42. https://doi.org/10.1016/j.aquaeng.2015.08.003.

Liu, Y., Liu, B., Lei, J., Guan, C., Huang, B., 2017a. Numerical simulation of the hydrodynamics within octagonal tanks in recirculating aquaculture systems. Chin. J. Oceanol. Limnol. 35 (4), 912–920. https://doi.org/10.1007/s00343-017-6051-3.

Liu, C., Yu, W., Chen, Z., Li, X., 2017b. Distributed polysquare mapping for large-scale semi-structured quad mesh generation. Comput. Aided Des. 90, 5–17. https://doi.org/10.1016/j.cad.2017.05.005.

Marshall, J.S., 2005. Particle dispersion in a turbulent vortex core. Phys. Fluids 17 (2), 025104. https://doi.org/10.1063/1.1829752.

Meshkov, E.E., Sirotkin, A.A., 2013. Bath-tub vortex attenuation with the increase of in-vessel water level. Physica Scripta 2013, 014058. https://doi.org/10.1088/0031-8949/2013/T155/014058.

Neipp, C., Hernández, A., Rodes, J.J., Márquez, A., Beléndez, T., Beléndez, A., 2003. An analysis of the classical Doppler effect. Eur. J. Phys. 24 (5), 497–505. https://doi.org/10.1088/0143-0807/24/5/306.

Ostermeier, P., Vandersickel, A., Gleis, S., Spliethoff, H., 2017. Three dimensional multi fluid modeling of Geldart B bubbling fluidized bed with complex inlet geometries. Powder Technol. 312, 89–102. https://doi.org/10.1016/j.powtec.2017.02.015.

Plew, D.R., Klebert, P., Rosten, T.W., Aspaas, S., Birkevold, J., 2015. Changes to flow and turbulence caused by different concentrations of fish in a circular tank. J. Hydraul. Res. 53 (3), 364–383. https://doi.org/10.1080/00221686.2015.1029016.

Pope, S.B., 2000. Turbulent Flows. Cambridge University Press.

Prabhu, P.A.J., Kaushik, S.J., Geuden, I., Stouten, T., Fontagné-dicharry, S., Veron, V., Mariojouls, C., Verreth, J.A.J., Eding, E.H., Schrama, J.W., 2017. Water exchange rate in RAS and dietary inclusion of micro-minerals influence growth, body composition and mineral metabolism in common carp. Aquaculture 471, 8–18. https://doi.org/10.1016/j.aquaculture.2016.12.031.

Prehn, J., Waul, C.K., Pedersen, L.F., Arvin, E., 2012. Impact of water boundary layer diffusion on the nitrification rate of submerged biofilter elements from a recirculating aquaculture system. Water Res. 46 (11), 3516–3524. https://doi.org/10.1016/j.watres.2012.03.053.

Pumir, A., Xu, H., Bodenschatz, E., Grauer, R., 2016. Single particle motion and vortex stretching in three dimensional turbulent flows. Phys. Rev. Lett. 116 (12), 124502. https://doi.org/10.1103/PhysRevLett.116.124502.

Sarrate, J., Ruiz-Girones, E., Roca, X., 2014. Unstructured and semi structured hexahedral mesh generation methods. Comput. Technol. Resour. 10, 35–64.

Schrottle, J., Dornbrack, A., Schumann, U., 2015. Excitation of vortex meandering in shear flow. Fluid Dyn. Res. 47 (3), 1–17. https://doi.org/10.1088/0169-5983/47/3/035508.

Shete, A.P., Verma, A.K., Chadha, N.K., Prakash, C., Peter, R.M., Ahmad, I., Nuwansi, K.K.T., 2016. Optimization of hydraulic loading rate in aquaponic system with Common carp (Cyrinus carpio) and Mint (Mentha arvensis). Aquacult. Eng. 72, 53–57. https://doi.org/10.1016/j.aquaeng.2016.04.004.

Shi, M.M., Ruan, Y.J., Li, J.P., Ye, Z.Y., Liu, G., Zhu, S.M., 2017. Numerical study of dense solid-liquid flow in hydrodynamic vortex separator applied in recirculating biofloc technology system. Aquacult. Eng. 79, 24–34. https://doi.org/10.1016/j.aquaeng.2017.08.002.

Stockton, K.A., Moffitt, C.M., Watten, B.J., Vinci, B.J., 2016. Comparison of hydraulics and particle removal efficiencies in a mixed cell raceway and Burrows pond rearing system. Aquacult. Eng. 74, 52–61. https://doi.org/10.1016/j.aquaeng.2016.04.005.

Summerfelt, S.T., Mathisen, F., Holan, A.B., Terjesen, B.F., 2016. Survey of large circular and octagonal tanks operated at Norwegian commercial smolt and post-smolt sites. Aquacult. Eng. 74, 105–110. https://doi.org/10.1016/j.aquaeng.2016.07.004.

Summerfelt, S.T., Davidson, J.W., Waldrop, T.B., Tsukuda, S.M., Williams, J.B., 2004. A partial reuse system for cold water aquaculture. Aquacult. Eng. 31 (3–4), 157–181. https://doi.org/10.1016/j.aquaeng.2004.03.005.

Tang, B., Xu, Y., Song, X., Sun, Z., Yu, J., 2017. Effect of inlet configuration on hydrocyclone performance. Trans. Nonferr. Metals Soc. China 27 (7), 1645–1655. https://doi.org/10.1016/S1003-6326(17)60187-0.

Terjesen, B.F., Summerfelt, S.T., Nerland, S., Ulgenes, Y., Fjæra, S.O., Reiten, B.K.M., Selset, R., Kolarevic, J., Brunsvik, P., Bæverfjord, G., Takle, H., Kittelsen, A.H., Åsgård, T., 2013. Design dimensioning, and performance of a research facility for studies on the requirements of fish in RAS environments. Aquacult. Eng. 54, 49–63.

https://doi.org/10.1016/j.aquaeng.2012.11.002.

Timmons, M.B., Summerfelt, S.T., Vinci, B.J., 1998. Review of circular tank technology and management. Aquacult. Eng. 18 (1), 51–69. https://doi.org/10.1016/S0144-8609(98)00023-5.

Uddin, E., Huang, W.-X., Sung, H.J., 2015. Actively flapping tandem flexible flags in a viscous flow. J. Fluid Mech. 780, 120–142. https://doi.org/10.1017/jfm.2015.460.

Venegas, P.A., Narvaez, A.L., Arriagada, A.E., Llancaleo, K.A., 2014. Hydrodynamic effects of use of eductors (Jet-Mixing Eductor) for water inlet on circular tank fish culture. Aquacult. Eng. 59, 13–22. https://doi.org/10.1016/j.aquaeng.2013.12.001.

Wang, S., Ohmura, N., 2017. Vortex Dynamics and Optical Vortices. In: Perez-de-Tejada, H. (Ed.), Vortex Dynamics and Optical Vortices. InTech Open Science, pp. 133–150.

Wright, N.G., Easom, G.J., 2003. Non-linear k–ε turbulence model results for flow over a building at full-scale. Appl. Math. Model. 27 (12), 1013–1033. https://doi.org/10.1016/S0307-904X(03)00123-9.

Xu, J., Shen, H., Wang, H., 2015. An industry-scale modeling for the turbulence agglomeration of fine particles. Adv. Mech. Eng. 7 (11), 1–10. https://doi.org/10.1177/1687814015617670.

Yang, F.L., Zhou, S.J., 2015. Free surface turbulent flow in an unbaffled stirred tank: Detached eddy simulation and VOF Study. Chem. Biol. Interact. Q. 29 (3), 395–403. https://doi.org/10.15255/CABEQ.2014.2056.

Zi, D., Wang, F.J., Yao, Z.F., Xiao, R.F., Chen, X., He, C.L., 2016. Numerical simulation on rectifying flow in intake system of a pumping station connected with headrace pipe. IOP Conf. Ser.: Earth Environ. Sci. 49, 032004. https://doi.org/10.1088/1755-1315/49/3/032004.